Journal of Physics: Conference Series **2156** (2022) 012023 doi:10.1088/1742-6596/2156/1/012023

Atomic Compton scattering effect on direct dark matter detection

Chang-Hao Fang[1,†,*], **Haitao Jia**[1], **Shin-Ted Lin**[1,‡]

[1] College of Physics, Sichuan University, Chengdu 6100000, China

[*] Speaker

E-mail: [†]fangch@stu.scu.edu.cn, [‡]stlin@scu.edu.cn

Abstract. Atomic Compton scattering effect significantly contributes to low-energy electronic recoils below its k-shell energy for the direct dark matter detection. Searches on ADM models, dark photon models, leptophilic dark matter models as well as the conventional WIMPs for background understandings are vitally required to clarify the effect. We employed the relativistic impulse approximation (RIA) together with the ab initio Multi-Configuration Dirac-Fock (MCDF) theory to obtain the atomic Compton scattering for Germanium (Ge) Silicon (Si) and Xenon (Xe) atoms. Comparisons on low momentum transfer regions with our calculations for Ge and Si are achieved. In addition, millicharged dark matter particles estimated by RIA in the atomic ionization for Ge and Xe have been evaluated. A factor-of-two discrepancy on the incoherent-scattering factor (a.k.a. scattering function) near 100 eV/c momentum transfer with the Ge system between our calculation and the latest version of `Geant4` (10.07.02) simulation data is observed. Plans on the experimental verification and the perspectives of the atomic Compton scattering effect for the direct detections will be discussed.

1. Introduction

Astronomical compelling evidence indicates that approximately 85% of the universe mass is made of the invisible dark matter. Hypothesis of Weakly Interacting Massive Particles (WIMPs) based on the current wisdom, turns out the lead candidate. However, the constantly null results from the direct dark matter detection experiments are motivated to consider the other possibilities. Models of axion and axion-like particles, dark photons, sterile neutrinos, etc give rise to the signature of the electron recoils (ER) rather than the nuclear recoils (NR) from the conventional WIMPs.

Atomic Compton scattering plays a key role in dark matter direct detection, as one of the crucial channels for ER and it contributes to the background in the low-energy region especially for which below K-shell ionization energy [1]. The latest `Geant4` [2] version adopts the results from Hubbel et al. [3] with impulse approximation (IA) or partially relativistic impulse approximation (RIA) [4], pointing out the insufficiency, in particular the background understanding at low-energy region associated while the direct-detection dark matter experiments are conducted.

In our work, a fully RIA method together with the electron wavefunction computed by an MCDF code is established and calculated. The scattering functions (SF) and their numerical results for elements including Ge, Si, Xe, and Ar, which are extensively employed as the detectors, are evaluated. Based on RIA, the low-energy spectrum for Ge is studied and

quantitively constructed. Simulations that obtained CDEX-1B and SuperCDMS detectors, with a revised `Geant4`, give energy spectrums in the low-energy region. Comparisons between theoretical and simulation results are analyzed. Besides, we show the RIA approach for another atomic ionization process caused by milli-charged particles, in which cross-sections and comparisons with other approaches are illustrated.

2. Fully RIA implementation

RIA developed by Ribberfors is widely used in atomic Compton scattering [5], since it involves atomic bonding and many-body effect into the scattering easily. In the point view of RIA, the electrons with momentum distribution scatter with incident photon independently, and the scattering process is so fast that the nuclear and other electrons are not influenced under such an impulse, i.e., electrons are treated as scattering from a momentum distribution invited by the atomic bound effect of free electrons. However, fully RIA implementation has not been taken yet. To get a more accurate calculation, an "exact" numerical method without using any further simplified approximations or factorization treatments is developed [6]. And comparisons with previous studies are made.

2.1. RIA: doubly differential cross section

The doubly differential cross-section (DDCS) of RIA can be written as

$$\left(\frac{d^2\sigma}{d\omega_f d\Omega_f}\right)_{\mathrm{RIA}} = \frac{r_0^2}{2}\frac{m_e}{q}\frac{\omega_f}{\omega_i}K_{\mathrm{KN}} \times \sum_{njl} Z_{njl}J_{njl}\left(p_z\right)\Theta\left(\omega_i - \omega_f - B_{njl}\right) \tag{1}$$

where r_0, m_e are classical radius and mass of electron respectively. q is the magnitude of momentum transfer in Compton scattering. ω_i, ω_f are the initial and final energy of photons. And Θ is the Heaviside step function. K_{XN} as a function of incoming and outgoing energy of photon represents for kinetic information of Klein-Nishina cross-section defined as follows

$$K_{\mathrm{KN}} = \frac{\omega_i}{\omega_f} + \frac{\omega_f}{\omega_i} - \sin^2\theta \tag{2}$$

The summation in Eq.1 means the DDCS sums over each sub-shell, in which $Z_{njl}, J_{njl}, B_{njl}$ correspond to the number of electrons, Compton profile, binding energy (or ionization energy) for each sub-shell respectively. θ is the scattering angle. The Compton profile represents electron momentum distribution along z-axis, defined as

$$J\left(p_z\right) \equiv \int \rho(\mathbf{p}) dp_x dp_y \tag{3}$$

Our atomic many-body calculation by MCDF updates the binding energy as well as the Compton profile simultaneously. Influences are revealed in the following discussions.

2.2. Differential cross-section and scattering function

The differential cross-section (DCS) is derived from Eq.1 by integrating over the whole energy space. According to the RIA approach, the DCS can be factorized into two parts

$$\left(\frac{d\sigma}{d\Omega_f}\right)_{\mathrm{RIA}} = \left(\frac{d\sigma}{d\Omega_f}\right)_{\mathrm{FEA}} \cdot SF(X) \tag{4}$$

The first term is Klein-Nishina cross-section under the free-electron approximation (FEA). The correcting term $SF(X)$ is the so-called scattering function, as a function of momentum transfer

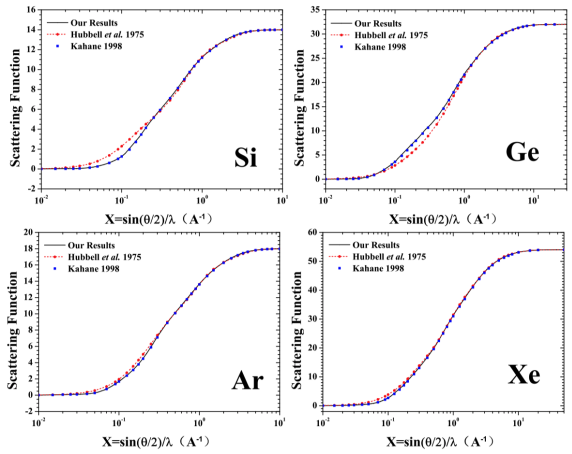

Figure 1. The numerical results of SFs. We illustrate the SF for Si, Ge, Ar, and Xe. We also presents the previous results [3].

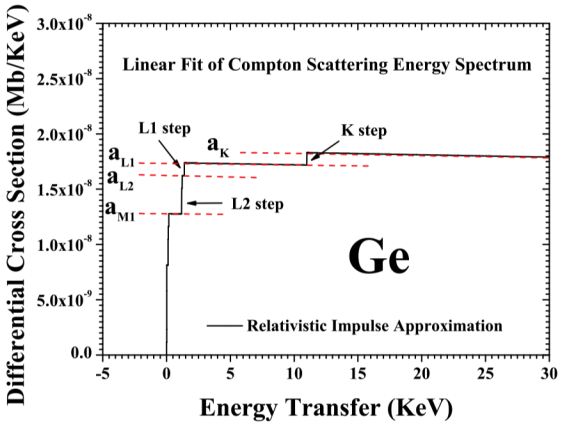

Figure 2. Demostration of the energy spectrum in the low-energy region. The step-like structures below K-shell ionization energy are illustrated emphatically.

X, in which, X is defined as $X = \sin\left(\frac{\theta}{2}\right)/\lambda\left[\mathring{A}^{-1}\right]$. In this sense, the SF can be interpreted as the number of effective free electrons for a binding system under a certain momentum transfer. By comparing Eq.4 with integrated Eq.1, we can derive the scattering function analytically

$$SF(\mathrm{X}) = \sum_{njl} Z_{njl}\Theta\left(\omega_i - \omega_f - B_{njl}\right)\int_{-\infty}^{p_{njl}^{\max}} dp_z J_{njl}\left(p_z\right). \tag{5}$$

The discrepancies show up when we compared our numerical scattering function with which deployed in the `Geant4` previously [3]. We illustrate a comparison between Hubbell's result and ours in Fig.1.

Fig.1 shows that there are notable discrepancies for Ge, Si, the semiconductor elements. Whereas, they match well for Ar and Xe, the inert elements. The reason for these discrepancies is due to the change of the binding energy and the Compton profile in Eq.5. The ideal to find the main reason that leads to these discrepancies is checking the binding energy and the atomic Compton profile separately. The comparisons of the atomic Compton profile between F. Biggs. et al.[7] and ours show the discrepancy appears at the higher momentum region but it has orders of magnitude lower than the dominant part. Integration over the momentum space of the Compton profile leads to a minor influence on the SF. Then, we use the MCDF ionization energy, Dirac-Fock Eigen-energy respectively to calculate the SF. Comparison between these results and Hubbell et al. [3] indicates the binding energies for each sub shell are the most influential part in the calculation of the SF. Thus we choose the practical binding energy data from the NIST database [8] in the following work. As illustrated in Table 1, our MCDF binding energies are the closest ones to the measurements, which reveals that the MCDF results are closer to what the atoms really are.

2.3. The low-energy spectrum

The Compton background directly depends on the shape of the low-energy spectrum, especially for that in the low-energy transfer or near photoionization threshold regions. Based on our RIA work, the Compton scattering energy spectrum for Ge in the low-energy region has been studied intensively [9].

Sub-shells	K	L_I	L_{IIa}	L_{IIb}	M_I	M_{II}
	$1s_{1/2}$	$2s_{1/2}$	$2p_{1/2}$	$2p_{3/2}$	$3s_{1/2}$	$3p_{1/2}$
	$1s$	$2s$	$2p^*$	$2p$	$3s$	$3p^*$
MCDF energy eigen state (eV)	11185.6	1454.5	1287.9	1255.6	201.5	144.8
MCDF ionization energy	11119.0	1426.9	1257.3	1226.0	193.3	136.8
Dirac-Fock ionization energy	10996.1	1398.4	1224.5	1177.8	183.5	127.4
Hartree-Fock ionization energy	11067.0	1402.3	1255.4	-	179.25	129.38
Measured binding energy	11103.1	1414.6	1248.1	1217.0	180.1	124.9

Table 1. Demonstration on ionization energy for $K - M_{II}$ sub-shells of Ge form theoretical calculations and measurements.

Our numerical result for Ge shows discontinuous, step-like structures below K-shell ionization energy, as illustrated in Fig. 2. Two parameters, slope and altitude, are assigned to describe these step structures, and a quantitive study for slopes and altitudes is carried out. The slopes got by both FEA and RIA are negative and the absolute values of slopes increase as reducing incident photon energy. The analyses for the altitudes of steps for different subshells are studied by considering relative altitude ratios. If energy transfer is larger than the K-shell ionization energy, all electrons can participate in the scattering process. However, once the energy transfer drops below the K-shell ionization energy, two electrons in $1s$ orbital would not be taken part in. If electrons in different subshells contribute equivalently in Compton scattering, the relative altitude ratio near K-shell ionization energy will be $30/32 = 0.94$. The numerical analyses for relative altitude ratios versus incident photon energy conclude that K and L shell electrons almost contribute equivalently in the Compton scattering energy spectrum, except for low incident photon energies.

2.4. Geant4 simulation and experimental design

In this section, we deployed our numerical result to `Geant4` simulation to involve detector geometry effect. The current `Geant4` simulation toolkit has included modules for low energy physics, such as `G4LowEPComptonModel` and `G4LivermoreCompton` [4].

Our work is involved when sampling the total cross-section, electron momentum distribution as well as photon scattering angle. In our simulation, the total cross-section, Compton profile, scattering function as well as ionization energy in `Geant4` are revised.

An experiment to inspect the discrepancies in the SF is designed. Detection is accessed with High Purity Germanium (HPGe) detector in the front and NaI detector in the end. Signals are identified to the Compton scattering if hits are captured in both detectors. The accessibility to our detection goal was examined by `Geant4` simulation. We adopted 662 keV gamma as the source and record information like energy, scattering angle, etc. In the low energy region, the simulated energy spectrums show notable discrepancies compared with the IA calculation in the DDCS implies a possibility to examine our theoretical results.

Besides, a simulation to study the relative altitude ratios of Compton step-like structures for Ge detectors in the low-energy region has been done. The geometries adopted in `Geant4` are CDEX-1B [10] and SuperCDMS [11] detector. These results match the theoretical ratios basically but reveal the influence of detector geometry does have affection on the low-energy spectrum [9].

2.5. RIA applied to milli-charged particles

The milli-charged particle is one of the beyond-standard-model particles regraded as a dark matter candidate. We demonstrate the RIA on milli-charged particles as an application in the

atomic ionization process [12]. With the RIA implementation, the cross-section for the ionization process has been derived.

In addition, numerical analysis has been taken. We compared our result with the previous approximation, free-electron approximation (FEA), and equivalent photon approximation (EPA). These two approximations validate in different energy regions, the FEA validates when energy transfer is large while the EPA validates when energy transfer is low. Our RIA approach matches well with FEA in the high energy transfer region as well as with EPA in the low energy transfer region.

3. Summary and prospects

The fully RIA with MCDF for Compton scattering is calculated and intensively studied for the low-energy regions. Notable differences in both SF and low-energy spectrum are revealed and studied with numerical analyses.

We plan to perform a promising experiment to clarify the discrepancy of SF at the low-energy regions. `Geant4` simulation with our calculations is successfully incorporated and available to compare the experiment with the geometry effect. Calculation and measurement of Compton scattering in the infrared divergence issue are ongoing.

4. Acknowledgement

This work was supported by the National Key Research and Development Program of China [2017YFA0402203], the National Natural Science Foundation of China [11975162], and the SPARK project from the research and innovation program of Sichuan University[2018SCUH0051].

References

[1] Barker D 2016 *arXiv:1611.05792 [astro-ph, physics:physics]* (*Preprint* `1611.05792`) URL `http://arxiv.org/abs/1611.05792`
[2] Agostinelli S *et al.* 2003 *Nuclear Instruments and Methods in Physics Research Section A: Accelerators, Spectrometers, Detectors and Associated Equipment* **506** 250–303
[3] Hubbell J H, Veigele W J, Briggs E A, Brown R T, Cromer D T and Howerton R J 1975 *Journal of Physical and Chemical Reference Data* **4** 471–538
[4] Brown J, Dimmock M, Gillam J and Paganin D 2014 *Nuclear Instruments and Methods in Physics Research Section B: Beam Interactions with Materials and Atoms* **338** 77–88
[5] Ribberfors R 1975 *Phys. Rev. B* **12** 2067–2074
[6] Qiao C K, Chi H C, Zhang L, Gu P, Liu C P, Tang C J, Lin S T and Huang K N 2020 *J. Phys. B: At. Mol. Opt. Phys.* **53** 075002
[7] Biggs F, Mendelsohn L and Mann J 1975 *Atomic Data and Nuclear Data Tables* **16** 201–309
[8] Hudson L 2003 X-ray Transition Energies, NIST Standard Reference Database 128
[9] Qiao C K, Chi H C, Lin S T, Gu P, Liu S K and Tang C J 2020 *J. Phys. G: Nucl. Part. Phys.* **47** 045202
[10] Jiang H *et al.* 2018 *Phys. Rev. Lett.* **120** 241301
[11] Agnese R *et al.* 2016 *Phys. Rev. Lett.* **116** 071301
[12] Qiao C K, Lin S T, Chi H C and Jia H T 2021 *J. High Energ. Phys.* **2021** 184